# We are IntechOpen, the world's leading publisher of Open Access books Built by scientists, for scientists

**4,800**
Open access books available

**122,000**
International authors and editors

**135M**
Downloads

Our authors are among the

**154**
Countries delivered to

**TOP 1%**
most cited scientists

**12.2%**
Contributors from top 500 universities

CLARIVATE ANALYTICS BOOK CITATION INDEX INDEXED

WEB OF SCIENCE™

Selection of our books indexed in the Book Citation Index in Web of Science™ Core Collection (BKCI)

## Interested in publishing with us?
## Contact book.department@intechopen.com

Numbers displayed above are based on latest data collected.
For more information visit www.intechopen.com

# 4

# Vortices in Electric Dipole Radiation

X. Li[1], D.M. Pierce[2] and H.F. Arnoldus[2]
[1]*California Polytechnic State University,*
[2]*Mississippi State University,*
*USA*

## 1. Introduction

In the geometrical optics limit of light propagation, light travels from a source to an observer along straight lines, known as optical rays. On the other hand, the energy in an electromagnetic field flows along the field lines of the Poynting vector. It can be shown (Born & Wolf, 1980) that in the geometrical optics limit, where variations in the radiation field on the scale of a wavelength are neglected, the optical rays coincide with the field lines of the Poynting vector, and both are straight lines. In nanophotonics and near-field optics, where sub-wavelength resolution of the energy transport is of interest, the optical rays lose their significance. Energy flows along the field lines of the Poynting vector, and these field lines are in general curves. When sub-wavelength resolution is required, we need the exact solution of Maxwell's equations. In order to study the fundamental aspects of energy propagation, we consider the simplest and most important source of radiation, which is the electric dipole. When a small object, like an atom, molecule or nanoparticle, is placed in an external electromagnetic field (usually a laser beam), oscillating with angular frequency $\omega$, a current will be induced in the particle, and this gives the particle an electric dipole moment of the form

$$\mathbf{d}(t) = d_{\mathrm{o}}\,\mathrm{Re}(\mathbf{u}\,e^{-i\omega t})\,, \tag{1}$$

with $d_{\mathrm{o}}$ an overall (real) constant, and $\mathbf{u}$ a complex-valued unit vector, normalized as $\mathbf{u}\cdot\mathbf{u}^{*}=1$. The oscillating dipole moment emits electromagnetic radiation. The electric field will have the form

$$\mathbf{E}(\mathbf{r},t) = \mathrm{Re}[\mathbf{E}(\mathbf{r})e^{-i\omega t}]\,, \tag{2}$$

with $\mathbf{E}(\mathbf{r})$ the complex amplitude, and the magnetic field $\mathbf{B}(\mathbf{r},t)$ has a similar form. We shall allow for the possibility that the dipole is embedded in a linear isotropic homogeneous medium with relative permittivity $\varepsilon_{\mathrm{r}}$ and relative permeability $\mu_{\mathrm{r}}$, and both are complex in general. The imaginary parts of $\varepsilon_{\mathrm{r}}$ and $\mu_{\mathrm{r}}$ are non-negative, as can be shown from causality arguments. The index of refraction $n$ of the medium is a solution of $n^2=\varepsilon_{\mathrm{r}}\mu_{\mathrm{r}}$, and we take the solution with $\mathrm{Im}\,n\geq 0$. When $\varepsilon_{\mathrm{r}}$ and $\mu_{\mathrm{r}}$ are both positive or both negative, we have $n^2>0$, and this leaves the sign of $n$ ambiguous. It can be shown with a limit procedure

(McCall et al., 2002) that we should take $n > 0$ when $\varepsilon_r$ and $\mu_r$ are both positive and $n < 0$ when $\varepsilon_r$ and $\mu_r$ are both negative. The time-averaged Poynting vector in such a medium is (Jackson, 1998)

$$\mathbf{S}(\mathbf{r}) = \frac{1}{2\mu_o}\mathrm{Re}\left[\frac{1}{\mu_r}\mathbf{E}(\mathbf{r})^* \times \mathbf{B}(\mathbf{r})\right] \tag{3}$$

## 2. Electric dipole radiation

Let the dipole be located at the origin of coordinates. The complex amplitudes of the electric and magnetic fields are then found to be (Li et al., 2011b)

$$\mathbf{E}(\mathbf{r}) = \frac{\mu_r d_o k_o^2}{4\pi\varepsilon_o}\left\{\mathbf{u} - (\hat{\mathbf{r}}\cdot\mathbf{u})\hat{\mathbf{r}} + [\mathbf{u} - 3(\hat{\mathbf{r}}\cdot\mathbf{u})\hat{\mathbf{r}}]\frac{i}{nk_o r}\left(1 + \frac{i}{nk_o r}\right)\right\}\frac{e^{ink_o r}}{r}\ , \tag{4}$$

$$\mathbf{B}(\mathbf{r}) = \frac{n\mu_r d_o k_o^2}{4\pi\varepsilon_o c}(\hat{\mathbf{r}}\times\mathbf{u})\left(1 + \frac{i}{nk_o r}\right)\frac{e^{ink_o r}}{r}\ , \tag{5}$$

for $\mathbf{r} \neq 0$ . Here, $k_o = \omega / c$ is the wavenumber of the radiation in free space and $\hat{\mathbf{r}} = \mathbf{r} / r$ is the unit vector in the radially outward direction. With these expressions for $\mathbf{E}(\mathbf{r})$ and $\mathbf{B}(\mathbf{r})$, the Poynting vector from (3) can be worked out. First we introduce

$$P_o = \frac{c d_o^2 k_o^4}{12\pi\varepsilon_o}\ , \tag{6}$$

which equals the power that would be emitted by the same dipole in free space. As we shall see, the field lines of the Poynting vector scale with $k_o$, so we introduce $\mathbf{q} = k_o\mathbf{r}$ as the dimensionless position vector of a field point. Similarly, we set $\bar{x} = k_o x$, etc., for the dimensionless Cartesian coordinates of a field point. Therefore, in dimensionless coordinates, a distance of $2\pi$ corresponds to one optical free-space wavelength. Then, the field lines of a vector field are determined by the directions of the vectors at each point in space, but not by their magnitudes. So when we set

$$\mathbf{S}(\mathbf{r}) = \frac{3P_o}{8\pi r^2}|\mu_r|^2\, e^{-2q\,\mathrm{Im}\,n}\boldsymbol{\sigma}(\mathbf{q})\ , \tag{7}$$

then the field lines of $\boldsymbol{\sigma}(\mathbf{q})$ are the same as the field lines of $\mathbf{S}(\mathbf{r})$, since the overall factor that is split off in (7) is positive. We shall simply refer to $\boldsymbol{\sigma}(\mathbf{q})$ as the Poynting vector. We find

$$\boldsymbol{\sigma}(\mathbf{q}) = [1 - (\hat{\mathbf{r}}\cdot\mathbf{u})(\hat{\mathbf{r}}\cdot\mathbf{u}^*)]\mathrm{Re}\left[\frac{n}{\mu_r}\left(1 + \frac{i}{nq}\right)\right]\hat{\mathbf{r}}$$

$$+\frac{1}{q|n|^2}\left|1 + \frac{i}{nq}\right|^2\{[1 - 3(\hat{\mathbf{r}}\cdot\mathbf{u})(\hat{\mathbf{r}}\cdot\mathbf{u}^*)]\mathrm{Im}(\varepsilon_r)\hat{\mathbf{r}} + 2\,\mathrm{Im}[\varepsilon_r(\hat{\mathbf{r}}\cdot\mathbf{u}^*)\mathbf{u}]\} \tag{8}$$

Vector $\boldsymbol{\sigma}(\mathbf{q})$ is dimensionless, and only depends on the field point through its dimensionless representation $\mathbf{q}$. It furthermore depends on the polarization vector $\mathbf{u}$ of the dipole moment, and it depends in a complicated way on the material parameters $\varepsilon_{\mathrm{r}}$ and $\mu_{\mathrm{r}}$.

## 3. Field lines of the poynting vector

A field line of the vector field $\boldsymbol{\sigma}(\mathbf{q})$ can be parametrized as $\mathbf{q}(u)$, with $u$ a dummy variable. Since at any point $\mathbf{q}$ on a field line the vector $\boldsymbol{\sigma}(\mathbf{q})$ is on the tangent line, the field lines are a solution of

$$\frac{\mathrm{d}\mathbf{q}}{\mathrm{d}u} = \boldsymbol{\sigma}(\mathbf{q}) \tag{9}$$

Given an initial point $\mathbf{q}_{\mathrm{i}}$, equation (9) determines the field line through this point. The dimensionless position vector $\mathbf{q}$ has Cartesian coordinates $(\bar{x},\bar{y},\bar{z})$, in terms of which (9) becomes

$$\frac{\mathrm{d}\bar{x}}{\mathrm{d}u} = \sigma_{\bar{x}}(\bar{x},\bar{y},\bar{z}) \ , \ \frac{\mathrm{d}\bar{y}}{\mathrm{d}u} = \sigma_{\bar{y}}(\bar{x},\bar{y},\bar{z}) \ , \ \frac{\mathrm{d}\bar{z}}{\mathrm{d}u} = \sigma_{\bar{z}}(\bar{x},\bar{y},\bar{z}) \tag{10}$$

Here, $\sigma_x(\bar{x},\bar{y},\bar{z})$ is the $x$ component of $\boldsymbol{\sigma}(\mathbf{q})$, expressed in the variables $\bar{x}$, $\bar{y}$ and $\bar{z}$. The field line pictures in this chapter are made by numerically integrating the set (10). For further analysis it is useful to express (9) in spherical coordinates $(q,\theta,\phi)$. This gives

$$\frac{\mathrm{d}q}{\mathrm{d}u} = \boldsymbol{\sigma}(\mathbf{q})\cdot\hat{\mathbf{r}} \ , \tag{11}$$

$$q\frac{\mathrm{d}\theta}{\mathrm{d}u} = \boldsymbol{\sigma}(\mathbf{q})\cdot\mathbf{e}_{\theta} \ , \tag{12}$$

$$q\sin\theta\frac{\mathrm{d}\phi}{\mathrm{d}u} = \boldsymbol{\sigma}(\mathbf{q})\cdot\mathbf{e}_{\phi} \tag{13}$$

At a large distance from the dipole, compared to a wavelength, we have $q >> 1$. Then the Poynting vector (8) simplifies to

$$\boldsymbol{\sigma}(\mathbf{q}) \approx [1-(\hat{\mathbf{r}}\cdot\mathbf{u})(\hat{\mathbf{r}}\cdot\mathbf{u}^*)]\mathrm{Re}\left(\frac{n}{\mu_{\mathrm{r}}}\right)\hat{\mathbf{r}} \tag{14}$$

It can be shown (McCall et al., 2002) that $\mathrm{Re}(n/\mu_r)$ is positive, and therefore the Poynting vector is approximately in the radially outward direction. We shall not consider the limiting case where $n/\mu_{\mathrm{r}}$ is imaginary. Therefore, at a large distance from the dipole the field lines are approximately straight lines, running away from the dipole. Conversely, any curving of the field lines can only occur close to the dipole, e.g., within a distance of about a wavelength. All terms in (8) are proportional to $\hat{\mathbf{r}}$, except for the term containing the factor $\mathrm{Im}[\varepsilon_{\mathrm{r}}(\hat{\mathbf{r}}\cdot\mathbf{u}^*)\mathbf{u}]$. Therefore, any curving of the field lines is due to this term. This can happen,

for instance, when **u** is complex, or when $\varepsilon_r$ has an imaginary part due to damping in the material.

## 4. Dipole in free space

Let us first consider a dipole in free space, so that $\varepsilon_r = \mu_r = n = 1$. The simplest case is when the incident field is linearly polarized, say along the $z$ axis. Then the dipole moment will oscillate along the $z$ axis, and we have $\mathbf{u} = \mathbf{e}_z$. With (1) we have

$$\mathbf{d}(t) = d_o \mathbf{e}_z \cos(\omega t) \tag{15}$$

The Poynting vector (8) becomes

$$\boldsymbol{\sigma}(\mathbf{q}) = \hat{\mathbf{r}} \sin^2\theta \ , \tag{16}$$

which is in the radially outward direction at all points. Therefore, the field lines are straight lines coming out of the dipole. Figure 1(a) shows the field line pattern.

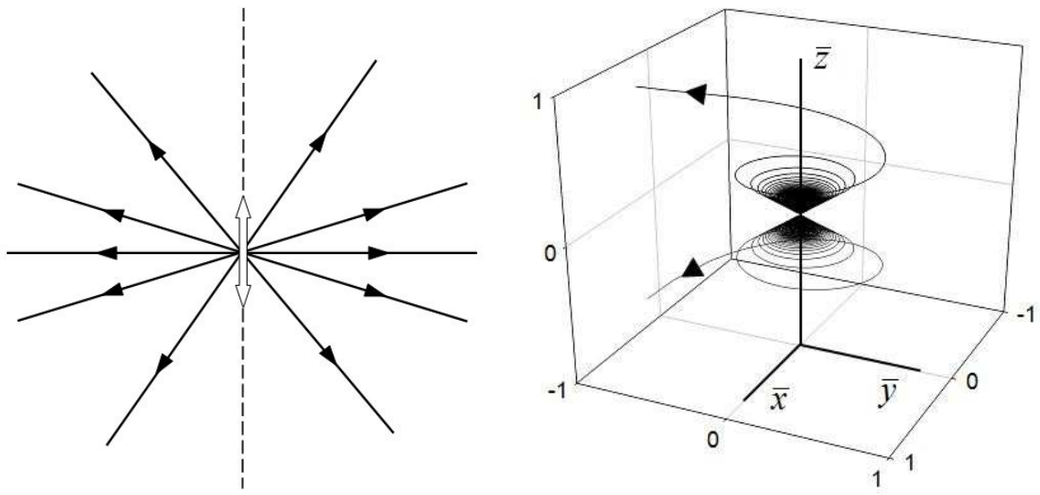


(a) (b)

Fig. 1. The figure on the left shows the field lines of the Poynting vector for a dipole which oscillates linearly in the direction of the arrow. In the figure on the right two field lines of the Poynting vector are shown for a dipole which rotates in the $xy$ plane. The field lines wind around the $z$ axis in the same direction as the direction of rotation of the dipole moment. The $x$ and $y$ axes in the figure have been lowered for clarity of drawing. The constant $\theta_o$ is $\pi/4$ for the upper field line, and this angle is the angle of the cone around the $z$ axis on which the field line runs. For the lower field line this angle is $3\pi/4$.

When the incident field is circularly polarized, with the electric field vector rotating in the $xy$ plane, the unit vector **u** is

$$\mathbf{u} = -\frac{1}{\sqrt{2}}(\mathbf{e}_x + i\mathbf{e}_y) \ , \tag{17}$$

and the dipole moment becomes

$$\mathbf{d}(t) = -\frac{d_{\mathrm{o}}}{\sqrt{2}}[\mathbf{e}_x \cos(\omega t) + \mathbf{e}_y \sin(\omega t)] \tag{18}$$

This dipole moment rotates in the *xy* plane, and the direction of rotation is counterclockwise when viewed down the positive *z* axis. The Poynting vector becomes

$$\boldsymbol{\sigma}(\mathbf{q}) = (1 - \tfrac{1}{2}\sin^2\theta)\hat{\mathbf{r}} + \frac{1}{q}\left(1 + \frac{1}{q^2}\right)\sin\theta\,\mathbf{e}_\phi \tag{19}$$

The first term on the right-hand side is in the radially outward direction, and the second term is proportional to $\mathbf{e}_\phi$. For *q* large, this second term vanishes, so at large distances, the field lines run radially outward. For small *q*, this second term dominates, and the field lines run approximately in the $\mathbf{e}_\phi$ direction. Since $\phi$ is the angle around the *z* axis, we expect the field lines to rotate around the *z* axis. Equations (11)-(13) for the field lines become

$$\frac{\mathrm{d}q}{\mathrm{d}u} = 1 - \tfrac{1}{2}\sin^2\theta \ , \tag{20}$$

$$\frac{\mathrm{d}\theta}{\mathrm{d}u} = 0 \ , \tag{21}$$

$$\frac{\mathrm{d}\phi}{\mathrm{d}u} = \frac{1}{q^2}\left(1 + \frac{1}{q^2}\right) \tag{22}$$

From (21) we see that $\theta$ is constant along a field line, and we shall indicate this constant by $\theta_{\mathrm{o}}$. Therefore, a field line lies on a cone with its axis as the *z* axis. Field lines run into the direction of increasing *u*, and since the right-hand side of (22) is positive, angle $\phi$ increases along a field line. Therefore, the field lines wind around the *z* axis in a counterclockwise direction when viewed down the positive *z* axis. From (22) and (20), and with $\theta = \theta_{\mathrm{o}}$, we have

$$\frac{\mathrm{d}\phi}{\mathrm{d}q} = Z(\theta_{\mathrm{o}})\frac{1}{q^2}\left(1 + \frac{1}{q^2}\right) \ , \tag{23}$$

where we have set

$$Z(\theta_{\mathrm{o}}) = \frac{1}{1 - \tfrac{1}{2}\sin^2\theta_{\mathrm{o}}} \tag{24}$$

We now see *q* as the independent variable, and then the solution of (23) is

$$\phi(q) = \phi_{\mathbf{o}} - Z(\theta_{\mathrm{o}})\frac{1}{q}\left(1 + \frac{1}{3q^2}\right) \ , \tag{25}$$

where $\phi_o$ is the integration constant. A field line starts at the location of the dipole, so at $q = 0$. The function $\phi(q)$ increases with $q$, and for $q \to \infty$ it reaches the asymptotic value of $\phi_o$. The field line spirals around the $z$ axis in the counterclockwise direction, when viewed down the positive $z$ axis, and this spiral lies on the cone $\theta = \theta_o$. Two field lines are shown in Fig. 1(b). The resulting field line picture has a vortex structure, and this was called '*the dipole vortex*' (Arnoldus & Foley, 2004). The spatial extent of this vortex is less than a wavelength, as can be seen from the figure. On this scale, a distance of $2\pi$ corresponds to one wavelength.

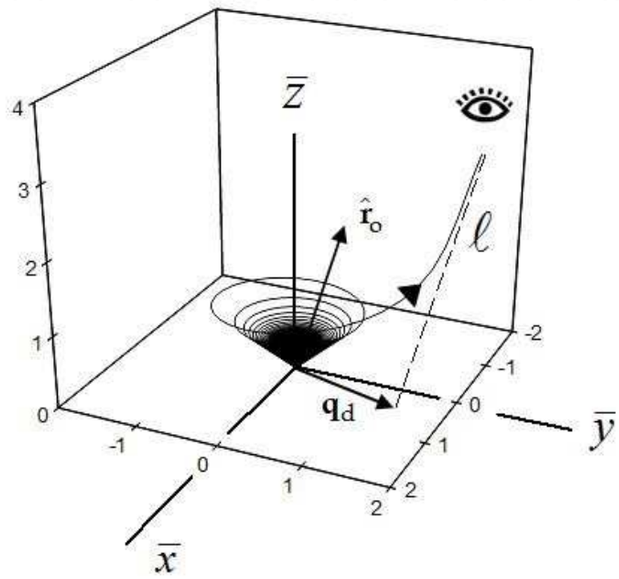


Fig. 2. A field line of the Poynting vector approaches asymptotically a line $\ell$ at a large distance from the source. This field line appears to come from a point in the $xy$ plane with position vector $\mathbf{q}_d$. Therefore, the dipole seems to be displaced over vector $\mathbf{q}_d$, when observed from the far field.

## 5. Virtual displacement of the source

For the circular dipole in free space, the field lines form a vortex structure, as illustrated in Fig. 1(b). Close to the source, the field lines wind around the $z$ axis numerous times, and then they run away to the far field, while remaining on a cone. In the far field, a field line approaches asymptotically a straight line, and this line is the optical ray from geometrical optics. In geometrical optics, a sub-wavelength spatial structure like the vortex is not resolved, and it would appear as if the optical ray comes from the location of the dipole. However, when sub-wavelength resolution is of interest, this is not the case anymore. Due to the rotation of a field line near the source, it appears as if the ray comes from a point in the $xy$ plane which is displaced with respect to the position of the dipole, as shown in Fig. 2. The line $\ell$ is the asymptote of the field line, and this is the optical ray. This line intersects the $xy$ plane at a location indicated by the displacement vector $\mathbf{q}_d$, so this vector represents the apparent location of the source.

The dimensionless Cartesian coordinates $(\bar{x},\bar{y},\bar{z})$ for a point on the field line are parametrized as

$$\bar{x} = q\sin\theta_{\mathrm{o}}\cos\phi(q) \ , \tag{26}$$

$$\bar{y} = q\sin\theta_{\mathrm{o}}\sin\phi(q) \ , \tag{27}$$

$$\bar{z} = q\cos\theta_{\mathrm{o}} \tag{28}$$

Here, $\theta_{\mathrm{o}}$ is the angle of the cone on which the field line lies, and $\phi(q)$ is given by (25). The free parameter is $q$. In order to obtain a representation of the line $\ell$, we expand the right-hand sides of (26)-(28) in an asymptotic series in $1/q$. Due to the overall factors of $q$, we need to expand $\cos\phi(q)$ and $\sin\phi(q)$ up to order $1/q$, so that the combination yields a constant. From (25) we have

$$\phi(q) = \phi_{\mathbf{o}} - \frac{1}{q}Z(\theta_{\mathrm{o}}) + \ldots \ , \tag{29}$$

and this gives

$$\cos\phi(q) = \cos\phi_{\mathrm{o}} + \frac{1}{q}Z(\theta_{\mathrm{o}})\sin\phi_{\mathrm{o}} + \ldots \ , \tag{30}$$

$$\sin\phi(q) = \sin\phi_{\mathrm{o}} - \frac{1}{q}Z(\theta_{\mathrm{o}})\cos\phi_{\mathrm{o}} + \ldots \tag{31}$$

Then we substitute the right-hand sides of (30) and (31) in (26) and (27), respectively, and omit the ellipses. We then obtain

$$\bar{x} = \sin\theta_{\mathrm{o}}[t\cos\phi_{\mathrm{o}} + Z(\theta_{\mathrm{o}})\sin\phi_{\mathrm{o}}] \ , \tag{32}$$

$$\bar{y} = \sin\theta_{\mathrm{o}}[t\sin\phi_{\mathrm{o}} - Z(\theta_{\mathrm{o}})\cos\phi_{\mathrm{o}}] \ , \tag{33}$$

$$\bar{z} = t\cos\theta_{\mathrm{o}} \tag{34}$$

Here we have replace $q$ by $t$, since this parameter does not represent the distance to the origin anymore. Equations (32)-(34) are the parameter equations for the line $\ell$. This line is the asymptote of the field line that runs into the observation direction $(\theta_{\mathrm{o}},\phi_{\mathrm{o}})$, and this direction is indicated by the eye in Fig. 2.

The unit vector in the observation direction $(\theta_{\mathrm{o}},\phi_{\mathrm{o}})$ is

$$\hat{\mathbf{r}}_{\mathrm{o}} = \sin\theta_{\mathrm{o}}(\cos\phi_{\mathrm{o}}\mathbf{e}_x + \sin\phi_{\mathrm{o}}\mathbf{e}_y) + \cos\theta_{\mathrm{o}}\mathbf{e}_z \ , \tag{35}$$

and the position vector of a point on the line is $\mathbf{q} = \bar{x}\mathbf{e}_x + \bar{y}\mathbf{e}_y + \bar{z}\mathbf{e}_z$. The parameter equations (32)-(34) can then be written in vector form as

$$\ell:\ \mathbf{q} = t\hat{\mathbf{r}}_\mathrm{o} + \mathbf{q}_\mathrm{d}\ , \tag{36}$$

where we have set

$$\mathbf{q}_\mathrm{d} = \sin\theta_\mathrm{o} Z(\theta_\mathrm{o})(\mathbf{e}_x \sin\phi_\mathrm{o} - \mathbf{e}_y \cos\phi_\mathrm{o}) \tag{37}$$

It follows from (34) that $\overline{z} = 0$ for $t = 0$, so the line $\ell$ intersects the *xy* plane for $t = 0$. From (36) we see that for $t = 0$ we have $\mathbf{q} = \mathbf{q}_\mathrm{d}$ so vector $\mathbf{q}_\mathrm{d}$ is the displacement vector from Fig. 2. From (35) and (37) it follows that $\mathbf{q}_\mathrm{d} \cdot \hat{\mathbf{r}}_\mathrm{o} = 0$, and therefore the displacement is perpendicular to the observation direction. The magnitude of the displacement vector is

$$q_\mathrm{d} = \frac{2\sin\theta_\mathrm{o}}{1 + \cos^2\theta_\mathrm{o}} \tag{38}$$

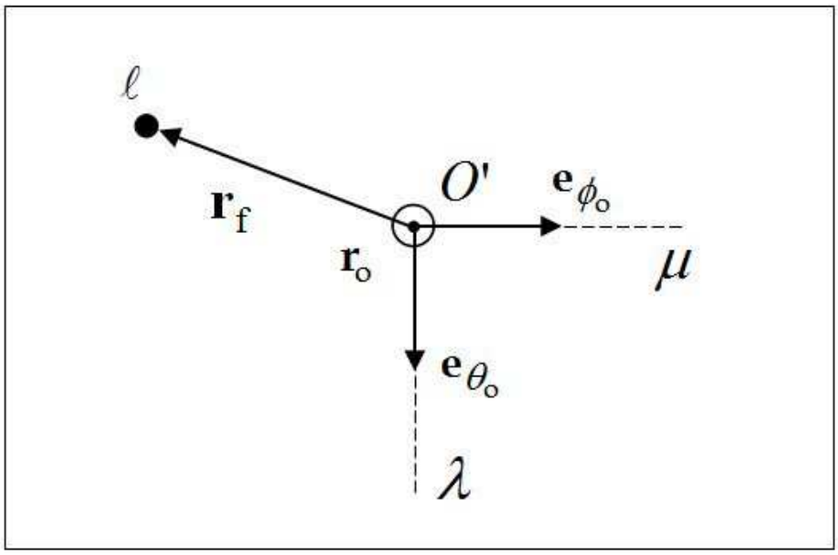


Fig. 3. Illustration of the image plane and the coordinate system in this plane.

The displacement is zero for observation along the *z* axis, and has its maximum for $\theta_\mathrm{o} = \pi/2$, e.g., for observation in the *xy* plane. The maximum displacement is $q_\mathrm{d} = 2$. Since $2\pi$ corresponds to one wavelength, this displacement equals $\lambda/\pi$, with $\lambda = 2\pi/k_\mathrm{o}$ the wavelength of the radiation. For visible light, this is of the order of about 150 nm. In nanophotonics, where structures with dimensions of a few nanometers are studied, this displacement is not negligible.

## 6. Displacement in the far field

In the far field, the line $\ell$ is the asymptote of the field line that runs into the observation direction $(\theta_\mathrm{o}, \phi_\mathrm{o})$. The virtual displacement of the source in the *xy* plane is then inferred from an extrapolation of the line $\ell$ from the far field to its intersection with the *xy* plane. We shall now consider this from a different point of view (Shu et al., 2008). For a given vector

$\mathbf{r}_o$, we define the observation plane, or image plane, as the plane which is perpendicular to $\mathbf{r}_o$, and which contains the point $\mathbf{r}_o$. We shall take the direction of $\mathbf{r}_o$ as specified by $(\theta_o, \phi_o)$, so that $\hat{\mathbf{r}}_o$ is given by (35). Therefore, we can view the image plane as the tangent plane of a sphere with radius $r_o$ around the dipole, and located at the spherical position $(\theta_o, \phi_o)$. So the position of the image plane is specified by its angular location $(\theta_o, \phi_o)$, and by its distance $r_o$ to the origin of coordinates. The point $\mathbf{r}_o$ is taken as the origin $O'$ in the plane, as illustrated in Fig. 3. The spherical-coordinate unit vectors $\mathbf{e}_{\theta_o}$ and $\mathbf{e}_{\varphi_o}$ lie in the image plane, and are given explicitly by

$$\mathbf{e}_{\theta_o} = (\mathbf{e}_x \cos\phi_o + \mathbf{e}_y \sin\phi_o)\cos\theta_o - \mathbf{e}_z \sin\theta_o \,, \tag{39}$$

$$\mathbf{e}_{\phi_o} = -\mathbf{e}_x \sin\phi_o + \mathbf{e}_y \cos\phi_o \tag{40}$$

We then introduce a $\lambda$ and a $\mu$ axis in the image plane, as shown in Fig. 3, so that a point in the image plane is represented by the Cartesian coordinates $(\lambda, \mu)$ in the plane. A point $\mathbf{r}$ in the image plane can therefore be written as

$$\mathbf{r} = \mathbf{r}_o + \lambda \mathbf{e}_{\theta_o} + \mu \mathbf{e}_{\phi_o} \tag{41}$$

A field line of the Poynting vector for the radiation emitted by a circular dipole in free space is parametrized by the angles $\theta_o$ and $\phi_o$, which are the asymptotic values of $\theta$ and $\phi$ along the field line. We now consider an image plane which is located at the angular location $(\theta_o, \phi_o)$, and we assume that the image plane is located in the far field, so $r_o$ is much larger than a wavelength of the radiation. Then the field line is approximately along the asymptote $\ell$. This line intersects the image plane at the location of the black dot in the figure. This point is represented by vector $\mathbf{r}_f$ in the image plane, as shown, or by the dimensionless vector $\mathbf{q}_f = k_o \mathbf{r}_f$. The parameter equation for $\ell$ is given by (36), and $\mathbf{q}_d$ can be written as

$$\mathbf{q}_d = -\sin\theta_o Z(\theta_o) \mathbf{e}_{\phi_o} \tag{42}$$

Since this is a vector in the image plane, we see immediately that

$$\mathbf{q}_f = \mathbf{q}_d \tag{43}$$

If the field lines were straight, then the field line in the $(\theta_o, \phi_o)$ direction would intersect the image plane at $O'$. Due to the rotation of the field lines, a field line intersects the image plane at $\mathbf{q}_f$, so $\mathbf{q}_f$ is the displacement of the field line in the far field. Apparently, this displacement is the same as the virtual displacement of the source in the $xy$ plane. This conclusion holds for a circular dipole in free space, but not in general, as we shall see below. The dimensionless coordinates in the image plane are $\bar{\lambda} = k_o \lambda$ and $\bar{\mu} = k_o \mu$. We then see from (42) that the intersection point of $\ell$ and the image plane has coordinates

$$\bar{\lambda}_f = 0 \,, \quad \bar{\mu}_f = -\sin\theta_o Z(\theta_o) \tag{44}$$

## 7. Image of the dipole

A single field line may not be directly observable by a detector. Usually, an image is formed on an image plane, and the intensity distribution over the plane is determined by a bundle of field lines that hit the plane. We shall take the plane of Fig. 3 as the image plane, and we consider the image formed on the plane by the radiation emitted by the circular dipole. Since $\hat{\mathbf{r}}_o$ is the unit normal on the plane, the intensity (power per unit area) at a point **r** on the plane is

$$I(\mathbf{r}_o;\lambda,\mu)=\mathbf{S}(\mathbf{r})\cdot\hat{\mathbf{r}}_o \tag{45}$$

The Poynting vector $\mathbf{S}(\mathbf{r})$ is evaluated at point **r** on the plane, with **r** written as in (41). The intensity depends on the position of the image plane, represented by $\mathbf{r}_o$. This position is determined by its angular location $(\theta_o,\phi_o)$ and by its distance $r_o$ to the dipole. We shall write $q_o=k_o r_o$ for the dimensionless representation of this distance. The dependence on $(\lambda,\mu)$ then gives the intensity distribution over the plane.

With the Poynting vector given by (7) and (19), the intensity distribution can be evaluated immediately. We obtain (Shu et al., 2009)

$$I(\mathbf{r}_o;\lambda,\mu)=I_o\left(\frac{q_o}{q}\right)^3\left\{1-\frac{1}{2q^2}[(q_o\sin\theta_o+\bar{\lambda}\cos\theta_o)^2+\bar{\mu}^2]-\frac{1}{q_o q}\left(1+\frac{1}{q^2}\right)\bar{\mu}\sin\theta_o\right\}, \tag{46}$$

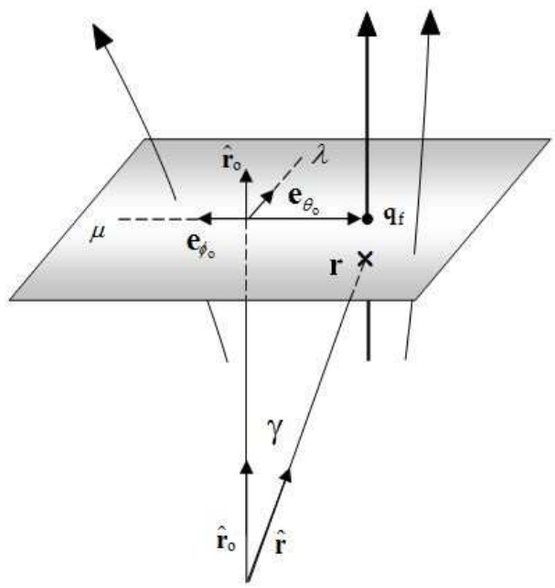


Fig. 4. The figure shows a 3D view of the image plane, the coordinate system, and several field lines. The bold field line is the field line that runs into the direction $(\theta_o,\phi_o)$ and it intersects the image plane under 90° if the image plane is located in the far field. Angle $\gamma$ is the angle under which the point **r** on the image plane is seen from the location of the dipole.

where we have set

$$q = \sqrt{q_o^2 + \bar{\lambda}^2 + \bar{\mu}^2} \ , \tag{47}$$

for the dimensionless distance between the point **r** in the image plane and the position of the dipole, and

$$I_o = \frac{3P_o}{8\pi r_o^2} \tag{48}$$

The overall factor $(q_o / q)^3$ has two contributions. A factor of $(q_o / q)^2$ comes from the fact that $\mathbf{S}(\mathbf{r})$ is proportional to $1/r^2$ and a factor of $q_o / q$ comes from the dot product of $\mathbf{S}(\mathbf{r})$ with $\hat{\mathbf{r}}_o$ in (45). So this comes from the projection of $\mathbf{S}(\mathbf{r})$ onto the normal direction, and therefore this factor accounts for the fact that a field line crosses the image plane under an angle other than 90°. We see form Fig. 4 that $q_o / q = \cos\gamma$, with $\gamma$ the angle under which the point **r** on the image plane is seen from the location of the dipole. An intensity distribution $I_o(q_o / q)^3$ would be a single peak at the origin of the image plane, and this peak is rotational symmetric around the normal vector $\hat{\mathbf{r}}_o$. The angular half-width at half maximum of the peak, as seen from the location of the dipole, would be 37°. The expression in braces in (46) accounts for the angular dependence of the emitted power and for the rotation of the field lines near the site of the dipole.

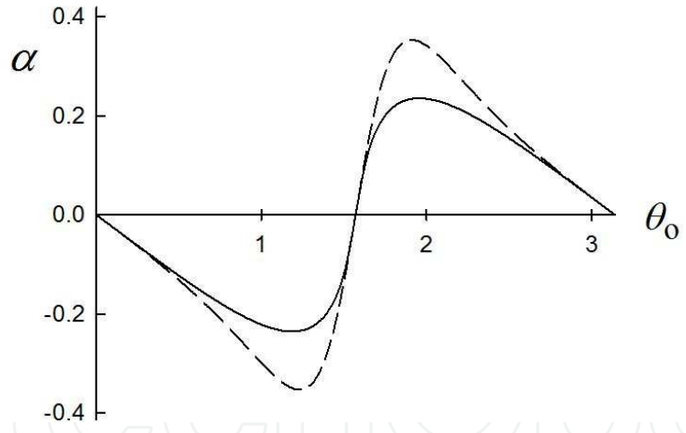


Fig. 5. The location of the peak of the intensity distribution is $(\bar{\lambda}_p, \bar{\mu}_p)$, and $\bar{\lambda}_p = \alpha q_o$. The solid line in the figure shows the dependence of $\alpha$ on $\theta_o$, and the dashed line is an approximation (Shu et al., 2009).

It can be shown that the intensity distribution (46) has a single peak in the $(\lambda, \mu)$ plane, when the image plane is located in the far field ($q_o >> 1$). Let $(\bar{\lambda}_p, \bar{\mu}_p)$ be the dimensionless coordinates of the position of the peak. If we write $\bar{\lambda}_p = \alpha q_o$, then $\alpha$ depends on the observation angle $\theta_o$, and can be computed numerically. The result is shown in Fig. 5. Since $\bar{\lambda}_p$ scales with $q_o$, the location of the peak in the $\bar{\lambda}$ direction is a result of the angular distribution of the radiated power, and not of the rotation of the field lines near the dipole. More interesting is the location of the peak in the $\bar{\mu}$ direction. We obtain

$$\bar{\mu}_{\mathrm{p}} = -(1+\alpha^2)^{3/2} \frac{2\sin\theta_{\mathrm{o}}}{8(1+\alpha^2) - 5(\sin\theta_{\mathrm{o}} + \alpha\cos\theta_{\mathrm{o}})^2} \tag{49}$$

This shift depends on $\theta_{\mathrm{o}}$, and this dependence is shown in Fig. 6. It is independent of $q_{\mathrm{o}}$, and it is a direct result of the rotation of the field lines near the source. The shift is maximum for $\theta_{\mathrm{o}} = \pi/2$, and the maximum shift is 2/3. Figure 7 shows the intensity distribution for this case.

The field line that runs into the $(\theta_{\mathrm{o}}, \phi_{\mathrm{o}})$ direction intersects the image plane at $\bar{\lambda}_{\mathrm{f}} = 0$ and

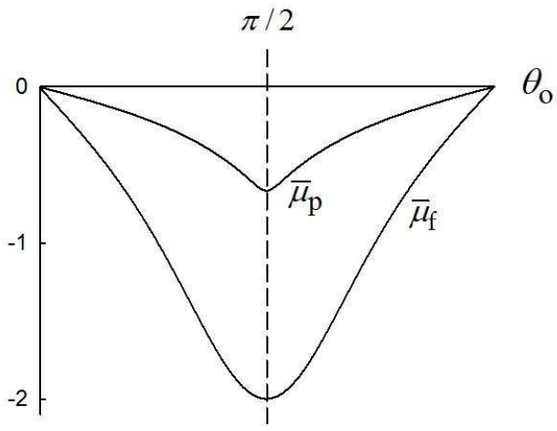


Fig. 6. The figure shows the dependence of $\bar{\mu}_{\mathrm{p}}$ and $\bar{\mu}_{\mathrm{f}}$ on $\theta_{\mathrm{o}}$.

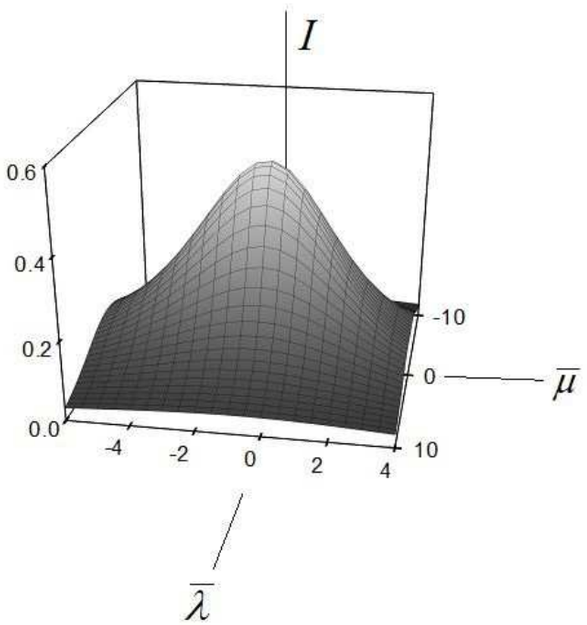


Fig. 7. The figure shows the intensity distribution over the image plane for $\theta_{\mathrm{o}} = \pi/2$. The coordinates of the peak are $(\bar{\lambda}_{\mathrm{p}}, \bar{\mu}_{\mathrm{p}}) = (0, -2/3)$, and this represents the largest possible shift from the origin due to the rotation of the field lines.

$$\bar{\mu}_{\mathrm{f}} = -\frac{2\sin\theta_{\mathrm{o}}}{1+\cos^2\theta_{\mathrm{o}}} \ , \tag{50}$$

according to (44). The value of $\bar{\mu}_{\mathrm{f}}$ is also shown in Fig. 6, and we see that it does not coincide with the location of the maximum of the intensity distribution. The displacement of the field line is larger than the shift of the peak of the profile. So, the displacement is a good indicator of the position of the image, but due to subtle effects the position of the image is not exactly at the same location where the field line for this $(\theta_{\mathrm{o}},\phi_{\mathrm{o}})$ direction intersects the image plane. Figure 8 illustrates how a bundle of field lines forms the image, rather than the field line for this direction only.

## 8. The difference profile

The shift of the peak in Fig. 7 is of the same order of magnitude as the spatial extent of the dipole vortex, and it is independent of the distance between the dipole and the observation plane, provided the image plane is in the far field. An experimental observation of this shift would confirm the existence of the vortex near the source. In this fashion, a property of the near field is observable through a measurement in the far field. However, the magnitude of the shift is less than a wavelength, and in the visible region of the spectrum, this is extremely small. Any observation of this shift would also require a very precise calibration of the experimental setup, since the shift is measured with respect to the origin $O'$ of the image plane. Furthermore, the profile has a large background, as can be seen from Fig. 7, and the shape of the background depends on the observation angle $\theta_{\mathrm{o}}$ .

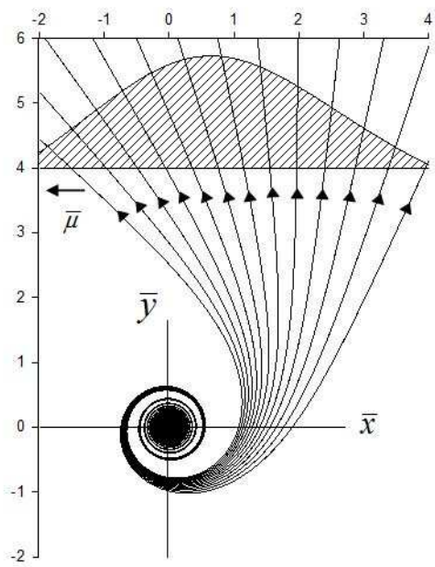


Fig. 8. The figure shows several field lines for a dipole that rotates counterclockwise in the $xy$ plane. The image plane here is located at $q_{\mathrm{o}} = 4$ , and at $\theta_{\mathrm{o}} = \phi_{\mathrm{o}} = \pi/2$ , so perpendicular to the $y$ axis. The field line in the $(\theta_{\mathrm{o}},\phi_{\mathrm{o}})$ direction intersects the image plane at $\bar{x} = 2$ and the maximum of the intensity profile is located at $\bar{x} = 2/3$ .

We see from Fig. 8 that the shift is due to the spiraling of the field lines. If we would reverse the rotation direction of the dipole, by reversing the helicity of the driving laser, the peak in the profile would move to $\bar{x} < 0$ in Fig. 8, and the background would remain approximately the same. When changing the direction of rotation of the dipole, expression (46) for the intensity remains the same, except that the term with $\bar{\mu}\sin\theta_o$ picks up a minus sign. We therefore introduce the difference profile $\Delta I$ as the intensity from (46) minus the same intensity for the radiation emitted by a dipole which rotates in the reverse direction. We then find (Li & Arnoldus, 2010a)

$$\Delta I(\mathbf{r}_o;\lambda,\mu) = -\frac{\zeta}{q^4}\left(1+\frac{1}{q^2}\right)\bar{\mu}\sin\theta_o \ , \tag{51}$$

where

$$\zeta = \frac{3P_o k_o^2}{4\pi} \tag{52}$$

In (51), $q$ is given by (47), so we see that $\Delta I$ depends on $q_o$, $\bar{\lambda}$ and $\bar{\mu}$. The dependence on the observation angle $\theta_o$ only enters through the overall factor $\sin\theta_o$. For a given $\theta_o$, the

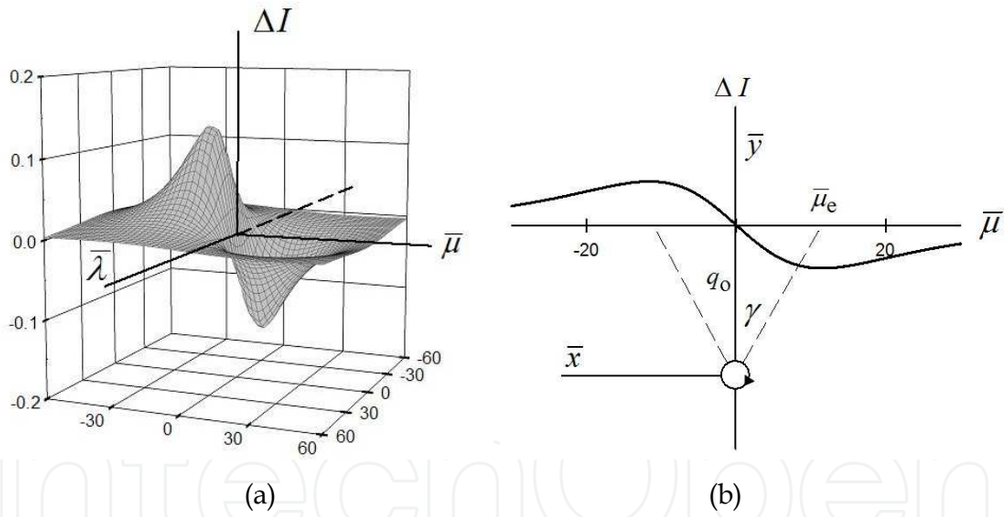


(a) (b)

Fig. 9. The figure on the left shows a 3D view of the intensity difference profile for $q_o = 20$, and the figure on the right shows the profile as a function of $\bar{\mu}$. The extrema have an angular location of $\gamma = 30^\circ$.

difference profile in the image plane is a function of $\bar{\lambda}$ and $\bar{\mu}$, with $q_o$ fixed. It is easily verified from (51) that $\Delta I$ has two extrema on the $\bar{\mu}$ axis, and since $\Delta I$ is antisymmetric in $\bar{\mu}$, there is a maximum and a minimum. This difference profile is shown in Fig. 9 for $q_o = 20$. The coordinates of the extrema are

$$\bar{\mu}_e = \pm\frac{q_o}{\sqrt{3}} \ , \tag{53}$$

for $q_o >> 1$, e.g., in the far field. The location of the peak in Fig. 7 is at $\bar{\mu} = -2/3$, and this is a displacement of about one-tenth of a wavelength with respect to $O'$. The extrema of the difference profile are proportional to $q_o$, and therefore these extrema are located at macroscopic distances from $O'$. As viewed from the dipole, they appear under an angle of $\gamma = 30^\circ$, as follows from (53). Therefore, the extrema in the difference profile are a macroscopic feature of the intensity distribution. They appear in the far field due to the rotation of the field lines in the near field. Even though the vortex is of microscopic dimension, the location of the peaks in $\Delta I$ is macroscopic. This opens the possibility to observe the dipole vortex through a measurement in the far field. Such an experiment was performed recently (Haefner et al., 2009). The small particles were polystyrene spheres with a diameter of 4.6 μm, the laser light had a wavelength of 532 nm and the observation angle was $\theta_o = 90^\circ$. The results of the experiment were in good agreement with Fig. 9(b).

## 9. Linear dipole in a medium

So far we have considered the radiation emitted by a dipole in free space. We shall now consider the effect of an embedding medium with relative permittivity $\varepsilon_r$ and relative permeability $\mu_r$, both of which are complex in general. When a plane electromagnetic wave travels through a material, say in the positive $z$ direction, then the magnitude of the Poynting vector decays exponentially along the direction of propagation. This magnitude is proportional to $\exp(-2k_o z \operatorname{Im} n)$, so energy is dissipated when the imaginary part of the index of refraction is finite. Since the field lines of the Poynting vector are determined by the direction of $\mathbf{S}(\mathbf{r})$, and not its magnitude, the damping by the material does not affect the field lines of the Poynting vector (which are straight lines, parallel to the $z$ axis, for this case). Let us now consider a linear dipole, oscillating along the $z$ axis. In free space, the Poynting vector is given by (16), and the field lines are straight lines, coming out of the dipole, as shown in Fig. 1(a). One may expect that the result of damping by the medium is a diminished power flow in the radially outward direction, but with a field line picture that is the same as in Fig. 1(a). This reduced power flow was already split off in (7) as the factor $\exp(-2q \operatorname{Im} n)$. We shall now show for dipole radiation the result of the damping is far more dramatic.

When we set $\mathbf{u} = \mathbf{e}_z$ in (8), we obtain for the Poynting vector

$$\boldsymbol{\sigma}(\mathbf{q}) = \hat{\mathbf{r}} \sin^2\theta \operatorname{Re}\left[\frac{n}{\mu_r}\left(1 + \frac{i}{nq}\right)\right]$$

$$+ \frac{1}{|n|^2 q}\left|1 + \frac{i}{nq}\right|^2 [\hat{\mathbf{r}}(1 - 3\cos^2\theta) + 2\mathbf{e}_z \cos\theta] \operatorname{Im} \varepsilon_r \qquad (54)$$

For a dipole in free space, this simplifies to $\boldsymbol{\sigma}(\mathbf{q}) = \hat{\mathbf{r}} \sin^2\theta$, giving field lines that run radially outward. When the dipole is embedded in a medium, this gets multiplied by Re[...]. It can be shown that this factor is positive (unless $n/\mu_r$ is imaginary, which we shall not consider here), and therefore this would still give field lines that run radially outward. Furthermore,

in the far field the second line in (54) vanishes, and we have $\boldsymbol{\sigma}(\mathbf{q}) \approx \hat{\mathbf{r}} \sin^2\theta \,\mathrm{Re}(n/\mu_\mathrm{r})$. So, in the far field, the field lines run approximately radially outward. When the imaginary part of $\varepsilon_\mathrm{r}$ is non-zero, the second line of (54) contributes to the Poynting vector. This term dominates in the near field, where $q$ is small, and it has a part which contains $\mathbf{e}_z$. This part is responsible for a deviation of the field lines from the radially outgoing pattern. Since this part only contributes when $\mathrm{Im}\,\varepsilon_\mathrm{r} \neq 0$, any deviation from the radial pattern is due to damping.

The vector field $\boldsymbol{\sigma}(\mathbf{q})$ from (54) is rotationally symmetric around the $z$ axis and reflection symmetric in the $xy$ plane. Therefore we only need to consider the field lines in the first quadrant of the $yz$ plane. In this quadrant, $\cos\theta$ is positive, and therefore the part of $\boldsymbol{\sigma}(\mathbf{q})$ containing $\mathbf{e}_z$ is in the positive $z$ direction. As a result, the field lines will bend away from the radial direction, and upward. The factor in square brackets in (54) is

$$\hat{\mathbf{r}}(1-3\cos^2\theta) + 2\mathbf{e}_z \cos\theta = \sin\theta[\mathbf{e}_y(1-3\cos^2\theta) + 3\mathbf{e}_z \sin\theta\cos\theta] \,, \tag{55}$$

from which we see that the $y$ component vanishes for $\cos\theta = 1/\sqrt{3}$, so $\theta = 54.7^\circ$. Therefore, when $\theta$ equals 54.7°, the part of the Poynting vector that contains $\mathrm{Im}\,\varepsilon_\mathrm{r}$ is in the positive $z$ direction. Consequently, the field lines in the near field cross the line $\theta = 54.7^\circ$ in a vertical, upward direction. Furthermore, for field points with a smaller angle $\theta$, the $y$ component of $\boldsymbol{\sigma}(\mathbf{q})$ is negative, and this means that the field line through such a point is headed towards the $z$ axis. At the $z$ axis we have $\theta = 0$, and it follows from (55) that the $z$ component vanishes, relative to the $y$ component, and therefore each field line in the near field approaches the $z$ axis under 90°. The resulting field line pattern is illustrated in Fig. 10.

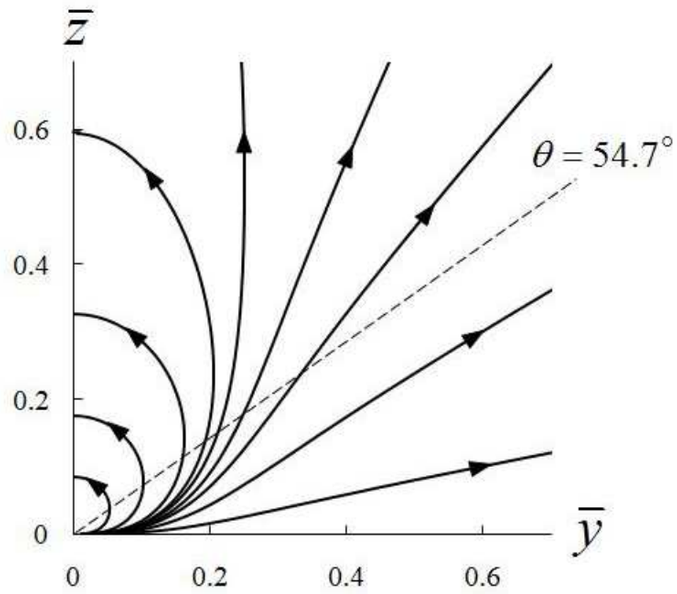


Fig. 10. The figure shows field lines of the Poynting vector for a dipole oscillating along the $z$ axis and embedded in a material with $\varepsilon_\mathrm{r} = 1.7 + 0.06i$ and $\mu_\mathrm{r} = 1$. These are the values for water at 3 μm. The index of refraction is $n = 1.3 + 0.023i$.

Interestingly, we see that very close to the dipole some field lines form semiloops. The energy that flows along such a semiloop comes out of the dipole and is then entirely dissipated by the material. The field line ends at the $z$ axis. A more careful analysis (Li et al., 2011a) shows that all field lines start off horizontally, so along the $xy$ plane. Therefore, all energy is initially emitted along the $xy$ plane. Some field lines form semiloops and some run to the far field where they eventually run approximately in the radial direction. This situation is in sharp contrast to the emission in free space, where the energy is emitted in all directions (except along the $z$ axis), as shown in Fig. 1(a). Another remarkable difference is the near the $z$ axis all field lines approach the $z$ axis under $90^{\text{o}}$, whereas for emission in free space the field lines near the $z$ axis run parallel to the $z$ axis.

When a linear dipole is embedded in a medium, the field lines of energy flow are curves, rather than straight lines, when the imaginary part of the relative permittivity is finite. Because of the damping, the energy flow is redistributed in the material. The effect of the dissipation is not only a weakening of the power transported along a field line, as for a plane wave, but the absorption during propagation results in a dramatic change in the direction of power flow in the near field.

## 10. Circular dipole in a medium

Let us now consider a rotating dipole moment, embedded in a medium. With $\mathbf{u}$ given by (17), the Poynting vector (8) becomes

$$\boldsymbol{\sigma}(\mathbf{q}) = \left(1-\tfrac{1}{2}\sin^2\theta\right)\mathrm{Re}\left[\frac{n}{\mu_{\mathrm{r}}}\left(1+\frac{i}{nq}\right)\right]\hat{\mathbf{r}}$$

$$+\frac{1}{|n|^2\,q}\left|1+\frac{i}{nq}\right|^2\left\{\left[\left(1-\tfrac{1}{2}\sin^2\theta\right)\hat{\mathbf{r}}+\tfrac{1}{2}\sin(2\theta)\mathbf{e}_\theta\right]\mathrm{Im}\,\varepsilon_{\mathrm{r}}+\mathbf{e}_\phi(\sin\theta)\,\mathrm{Re}\,\varepsilon_{\mathrm{r}}\right\} \tag{56}$$

The right-hand side of the first line of (56) is proportional to $\hat{\mathbf{r}}$. This is the leading term in the far field, so far from the dipole the field lines run approximately in the radially outward direction. The term on the second line of (56) has a part proportional to $\mathbf{e}_\phi(\sin\theta)\,\mathrm{Re}\,\varepsilon_{\mathrm{r}}$, and if the imaginary part of $\varepsilon_{\mathrm{r}}$ is zero, this is the only additional term. In that case, the Poynting vector has no $\mathbf{e}_\theta$ component, and therefore $\theta$ is constant along a field line, according to (12). Consequently, a field line lies on a cone around the $z$ axis, as in Fig. 1(b) for $\varepsilon_{\mathrm{r}}=1$. When there is damping in the material due to the imaginary part of $\varepsilon_{\mathrm{r}}$, the vector $\boldsymbol{\sigma}(\mathbf{q})$ has an $\mathbf{e}_\theta$ component. This will lead to a redirection of the field lines, and hence the field lines will not lie on a cone anymore. In other words, the flow of energy will be redistributed due to the damping, just like in the previous section.

The field line equations (11)-(13) become with (56)

$$\frac{\mathrm{d}q}{\mathrm{d}u} = g(q,\theta)\ , \tag{57}$$

$$\frac{\mathrm{d}\theta}{\mathrm{d}u} = \frac{1}{2\,|n|^2\,q^2}\left|1+\frac{i}{nq}\right|^2\sin(2\theta)\,\mathrm{Im}\,\varepsilon_{\mathrm{r}}\ , \tag{58}$$

$$\frac{\mathrm{d}\phi}{\mathrm{d}u} = \frac{1}{|n|^2\, q^2}\left|1+\frac{i}{nq}\right|^2 \mathrm{Re}\,\varepsilon_\mathrm{r} \ , \tag{59}$$

with

$$g(q,\theta) = \left(1-\tfrac{1}{2}\sin^2\theta\right)\left\{\mathrm{Re}\left[\frac{n}{\mu_\mathrm{r}}\left(1+\frac{i}{nq}\right)\right]+\frac{1}{|n|^2\, q}\left|1+\frac{i}{nq}\right|^2 \mathrm{Im}\,\varepsilon_\mathrm{r}\right\} \tag{60}$$

A field line runs into the direction of increasing $u$. Since $\mathrm{Im}\,\varepsilon_\mathrm{r} \geq 0$, the function $g(q,\theta)$ is positive, and it then follows from (57) that $q$ increases without bounds along a field line. Therefore, field lines start at the dipole, and run away to the far field. For the linear dipole, some field lines form semiloops, as seen in Fig. 10, but for a circular dipole this can not happen. For $q$ large, the right-hand sides of (58) and (59) vanish, and therefore angles $\theta$ and $\phi$ for points on a field line approach the constant values $\theta_\mathrm{o}$ and $\phi_\mathrm{o}$, just like in section 4 for the circular dipole in free space. Therefore, field lines approach asymptotically a straight line $\ell$, as illustrated in Fig. 11.

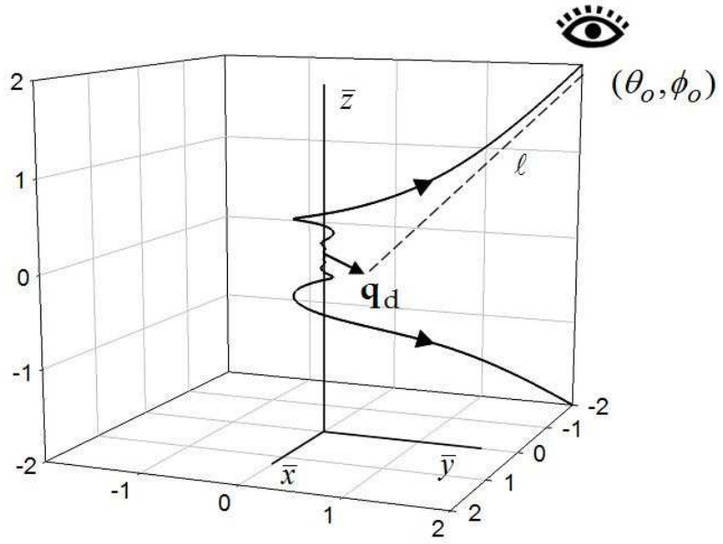


Fig. 11. Two field lines of the Poynting vector for a rotating dipole moment, embedded in a material with $\varepsilon_\mathrm{r} = 1+0.2i$ and $\mu_\mathrm{r} = 1$. Field lines approach asymptotically a straight line, and this gives rise to a virtual displacement $\mathbf{q}_\mathrm{d}$ of the source.

### 10.1 Rotation of the field lines

Angle $\phi$ is the angle around the $z$ axis, and we see from (59) that $\mathrm{d}\phi/\mathrm{d}u$ is positive when $\mathrm{Re}\,\varepsilon_\mathrm{r}$ is positive. Then $\phi$ increases along a field line, and the field line swirls around the $z$ axis in the counterclockwise direction when viewed down the $z$ axis. However, when $\mathrm{Re}\,\varepsilon_\mathrm{r}$ is negative, angle $\phi$ decreases along a field line, and the field line rotates clockwise around the $z$ axis. In this case, the direction of rotation of the field lines is opposite to the direction of rotation of the dipole moment. A material with $\mathrm{Re}\,\varepsilon_\mathrm{r} < 0$ (and $\mu_\mathrm{r} = 1$) is metallic, and the

index of refraction is approximately imaginary. We see from (7) that this gives a very strong damping in the medium, and therefore hardly any radiation will be emitted. However, for materials known as double negative metamaterials the real part of the permeability is also negative, and then the index of refraction becomes approximately real (and negative). In that case the material is transparent, and the dipole radiation can propagate away from the site of the source with little damping. Among the many peculiar features of these metamaterials, this reversal of rotation of the dipole vortex is certainly noteworthy (Li & Arnoldus, 2010c).

Because $q$ increases monotonically along a field line, we can consider $q$ as the independent variable rather than $u$. We then find from (57)-(59)

$$\frac{\mathrm{d}\theta}{\mathrm{d}q} = \frac{1}{g(q,\theta)} \frac{1}{2|n|^2 q^2} \left| 1 + \frac{i}{nq} \right|^2 \sin(2\theta) \operatorname{Im} \varepsilon_{\mathrm{r}} \ , \tag{61}$$

$$\frac{\mathrm{d}\phi}{\mathrm{d}q} = \frac{1}{g(q,\theta)} \frac{1}{|n|^2 q^2} \left| 1 + \frac{i}{nq} \right|^2 \operatorname{Re} \varepsilon_{\mathrm{r}} \tag{62}$$

Let us now consider the solution for $q$ small. For $\operatorname{Im} \varepsilon_{\mathrm{r}} = 0$ we see from (61) that $\theta$ is constant, and so a field line lies on a cone. Then we expand the right-hand side of (62) for $q$ small, and integrate. This yields

$$\phi(q) = \begin{cases} O\left(1/q^3\right) & , \quad \operatorname{Im} \mu_{\mathrm{r}} = 0 \\ O\left(1/q^2\right) & , \quad \operatorname{Im} \mu_{\mathrm{r}} \neq 0 \end{cases} \tag{63}$$

For $q \to 0$, the value of $\phi(q)$ goes to $\infty$ or $-\infty$ very quickly, and this leads to a large number of rotations of a field line around the $z$ axis, as can be seen in Fig. 1(b). For $\operatorname{Im} \varepsilon_{\mathrm{r}} \neq 0$ we find in a similar way

$$\phi(q) = \begin{cases} \dfrac{2}{\alpha} \ln q + O(1) & , \quad z = 0 \\ \dfrac{1}{\alpha} \ln q + O(1) & , \quad z \neq 0 \end{cases} , \tag{64}$$

where we have set

$$\alpha = \frac{\operatorname{Im} \varepsilon_{\mathrm{r}}}{\operatorname{Re} \varepsilon_{\mathrm{r}}} \tag{65}$$

For $\operatorname{Im} \varepsilon_{\mathrm{r}} \neq 0$, the approach of $\phi(q)$ to $\pm\infty$ is logarithmic, so much slower than for the case $\operatorname{Im} \varepsilon_{\mathrm{r}} = 0$. Consequently, the windings around the $z$ axis are much thinner than in Fig. 1(b). Due to the damping, it appears as if the field lines wind around the $z$ axis only a few times, as can be seen in Figs. 11 and 12.

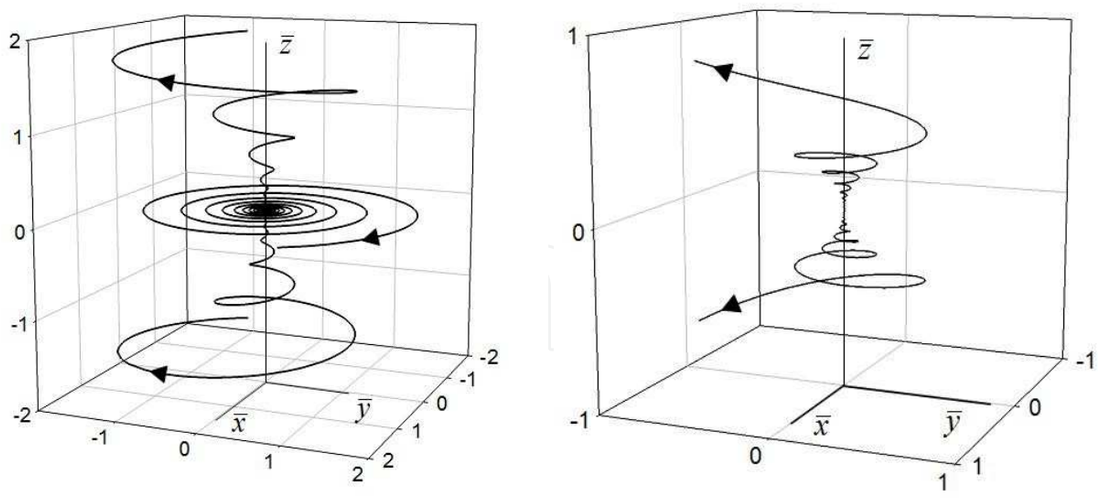


(a) (b)

Fig. 12. The figure on the left shows two field lines of the Poynting vector for $\varepsilon_r = -1 + 0.1i$ and $\mu_r = 1$. We see that the direction of rotation is reversed, as compared to the direction of rotation in Fig. 1(b). The figure on the right shows two field lines of the Poynting vector for $\varepsilon_r = 1 + 0.07i$ and $\mu_r = 1$. The field lines swirl around on a funnel surface, rather than a cone.

### 10.2 The funnel vortex

When $\mathrm{Im}\,\varepsilon_r = 0$, field lines lie on a cone, as in Fig. 1(b), and they are very dense near the location of the dipole. We see from Figs. 11 and 12 that when $\mathrm{Im}\,\varepsilon_r \neq 0$ the field lines are not only less dense near the source, but they also do not lie on a cone anymore. We see from the figures that due to the damping the field lines now lie on a funnel-shape surface. It follows from (62) that $\phi$ increases or decreases monotonically along a field line. We shall now consider $\phi$ as the independent parameter, and we consider $\theta$ to be a function of $\phi$. From (61) and (62) we then find

$$\frac{\mathrm{d}\theta}{\mathrm{d}\phi} = \tfrac{1}{2}\alpha \sin(2\theta) \ . \tag{66}$$

The solution of this equation is

$$\tan\theta = e^{\alpha(\phi-\phi_i)} \tan\theta_i \ , \tag{67}$$

with $(\theta_i, \phi_i)$ coordinates of the initial point. We now consider again the behavior of a field line for $q \to 0$, when $\mathrm{Im}\,\varepsilon_r \neq 0$. It follows from (64) that $\phi \to -\infty$ for $\alpha > 0$, and to $\infty$ for $\alpha < 0$, in the limit $q \to 0$. Therefore, $\alpha\phi \to -\infty$ in both cases, and so $\tan\theta \to 0$ for $q \to 0$. If the initial point is in the region $z > 0$, so $0 < \theta_i < \pi/2$, this implies that $\theta \to 0$ for $q \to 0$. Similarly, if $\pi/2 < \theta_i < \pi$ we have $\theta \to \pi$. For an initial point in the $xy$ plane we have $\theta_i = \pi/2$, and it follows from (58) that then $\theta = \pi/2$ for all points along the field line.

Therefore, the field line lies in the *xy* plane. It follows from (64) and (67) that $\tan\theta = O(q)$ for $\theta_\mathrm{i} \neq \pi/2$. Consequently, we have for $q \to 0$

$$\theta(q) = \begin{cases} O(q) & , \quad z > 0 \\ \pi/2 & , \quad z = 0 \\ \pi + O(q) & , \quad z < 0 \end{cases} \tag{68}$$

It follows from (68) that $\theta = 0$, $\theta = \pi/2$ or $\theta = \pi$ for $q \to 0$. Because the radiated energy is emitted along a field line, we come to the remarkable conclusion that due to the damping all energy is emitted along the *z* axis or along the *xy* plane, and this is illustrated in Fig. 12(a). This is in sharp contrast to the situation for $\mathrm{Im}\,\varepsilon_\mathrm{r} = 0$, because then field lines lie on any cone around the *z* axis. In that case, the energy is emitted into the direction $\theta_\mathrm{o}$, with $\theta_\mathrm{o}$ the angle of the cone.

### 10.3 The displacement

As shown in Fig. 11, a field line approaches asymptotically a straight line $\ell$ in the far field. The field line runs in the $(\theta_\mathrm{o}, \phi_\mathrm{o})$ direction, but the line $\ell$ does not go through the origin of coordinates. In order to find the line $\ell$, we expand the right-hand sides of (61) and (62) in a series in $1/q$, and integrate the result. We then obtain

$$\theta(q) = \theta_\mathrm{o} - Z(\theta_\mathrm{o}) \frac{\sin(2\theta_\mathrm{o})}{2q} \mathrm{Im}\,\varepsilon_\mathrm{r} + \ldots \,, \tag{69}$$

$$\phi(q) = \phi_\mathrm{o} - Z(\theta_\mathrm{o}) \frac{1}{q} \mathrm{Re}\,\varepsilon_\mathrm{r} + \ldots \,, \tag{70}$$

where

$$Z(\theta_\mathrm{o}) = \frac{1}{|n|^2\, \mathrm{Re}(n/\mu_\mathrm{r}) \left(1 - \frac{1}{2}\sin^2\theta_\mathrm{o}\right)} \tag{71}$$

Along similar steps as in section 5, we now find

$$\ell : \ \mathbf{q} = t\hat{\mathbf{r}}_\mathrm{o} + \mathbf{q}_\mathrm{f} \,, \tag{72}$$

with

$$\mathbf{q}_\mathrm{f} = -\sin\theta_\mathrm{o} Z(\theta_\mathrm{o}) [\mathbf{e}_{\phi_\mathrm{o}} \mathrm{Re}(\varepsilon_\mathrm{r}) + \mathbf{e}_{\theta_\mathrm{o}} \cos\theta_\mathrm{o} \mathrm{Im}(\varepsilon_\mathrm{r})] \tag{73}$$

Vector $\mathbf{q}_\mathrm{f}$ is perpendicular to $\hat{\mathbf{r}}_\mathrm{o}$, so it is a vector in the image plane. It represents the displacement in the far field, and it corresponds to the intersection of $\ell$ with the image plane, as in Fig. 3. For a dipole in free space, the virtual displacement in the *xy* plane, $\mathbf{q}_\mathrm{d}$, is the same as the displacement $\mathbf{q}_\mathrm{f}$ of a field line in the far field. With damping, this is not the case anymore. The intersection of $\ell$ with the *xy* plane is now found to be

$$\mathbf{q}_{\mathrm{d}} = -\sin\theta_{\mathrm{o}} Z(\theta_{\mathrm{o}})[\mathbf{e}_{\phi_{\mathrm{o}}} \mathrm{Re}(\varepsilon_{\mathrm{r}}) + \mathbf{e}_{\rho_{\mathrm{o}}} \mathrm{Im}(\varepsilon_{\mathrm{r}})] \ , \tag{74}$$

with

$$\mathbf{e}_{\rho_{\mathrm{o}}} = \mathbf{e}_x \cos\phi_{\mathrm{o}} + \mathbf{e}_y \sin\phi_{\mathrm{o}} \ , \tag{75}$$

the radially outward unit vector in the *xy* plane. The magnitude of the displacement is

$$q_{\mathrm{d}} = \frac{2\sin\theta_{\mathrm{o}}}{|\mu_{\mathrm{r}}|\,\mathrm{Re}(n/\mu_{\mathrm{r}})(1+\cos^2\theta_{\mathrm{o}})} \ , \tag{76}$$

which generalizes (38). In free space, the maximum value of $q_d$ is 2, and this occurs for $\theta_{\mathrm{o}} = \pi/2$. For a dipole embedded in a material, the factor $\mathrm{Re}(n/\mu_{\mathrm{r}})$ in the denominator can become small, and this would give a large $q_d$. This could happen, for instance, for $\mu_{\mathrm{r}} = 1$ and $\varepsilon_{\mathrm{r}}$ approximately negative. Then $n$ is approximately imaginary, and the displacement is very large.

## 11. Linear dipole near a mirror

We have studied the field lines of energy flow for an electric dipole with a linear and a rotating dipole moment, both in free space and in an embedding medium. In this section we shall consider the effect of the presence of a boundary. Let the dipole be located on the *z* axis, a distance *H* above a mirror. The surface of the mirror is taken as the *xy* plane. We shall consider a linear dipole, oscillating under an angle $\gamma$ with the *z* axis, so

$$\mathbf{u} = \mathbf{e}_y \sin\gamma + \mathbf{e}_z \cos\gamma \tag{77}$$

In the region $z > 0$ the field is identical to the field of the dipole plus the field of its mirror image (which is the reflected field at the interface). The mirror dipole is located a distance *H* below the *xy* plane, and it has a dipole moment represented by

$$\mathbf{u}^{\mathrm{im}} = -\mathbf{e}_y \sin\gamma + \mathbf{e}_z \cos\gamma \tag{78}$$

The setup is shown in Fig. 13. Let $\mathbf{r}_1$ be the location of a field point, measured from the location of the dipole, and $\mathbf{r}_2$ be the same field point but measured from the image dipole. The electric and magnetic field amplitudes are then given by (4) and (5) with $\mathbf{r}$ replaced by $\mathbf{r}_1$, and for the amplitudes of the image fields we replace $\mathbf{r}$ by $\mathbf{r}_2$ and $\mathbf{u}$ by $\mathbf{u}^{\mathrm{im}}$. The Poynting vector can then be constructed, and field lines can be drawn with the method outlined in section 3 (Li & Arnoldus, 2010b). Figure 14 shows the field lines for a perpendicular ($\gamma = 0$) and a parallel ($\gamma = \pi/2$) dipole, both for $h = k_{\mathrm{o}} H = 2\pi$. For these cases, the field line patterns are rotationally symmetric around the *z* axis. Without the interface, the field lines are straight, as in Fig. 1(a). For the perpendicular dipole, Fig. 14(a), the field lines are more or less straight near the dipole. The field lines that run

towards the mirror bend at the mirror, and then run off more or less horizontally. For the parallel dipole, Fig. 14(b), the pattern is much more complex. We see that singularities appear, which are indicated by small white circles. At such a singularity the Poynting vector vanishes. We see from the figure that several field lines end at a singularity, and other field lines bend such as to avoid the singularity. The case of $\gamma = 45^\circ$ is shown in Fig. 15. The field line pattern is not rotationally symmetric around the $z$ axis anymore. At the right of the $z$ axis, the pattern is similar to Fig. 14(a). On the left of the $z$ axis we see numerous singularities, and we now also observe the appearance of three optical vortices in the energy flow pattern. The points labeled *a*, *b* and *c* in the figure are singularities at the centers of the vortices. At the other singularities, except for *d*, field lines abruptly change direction. It is also interesting to see that there are field lines which start at point *a* and end at point *b*. These field lines represent a local energy flow where the energy does not directly originate from the location of the dipole. At point *e*, some field lines seem to collide, and this leads to a singularity. At singularities *f*, *g* and *h*, field lines split in two directions.

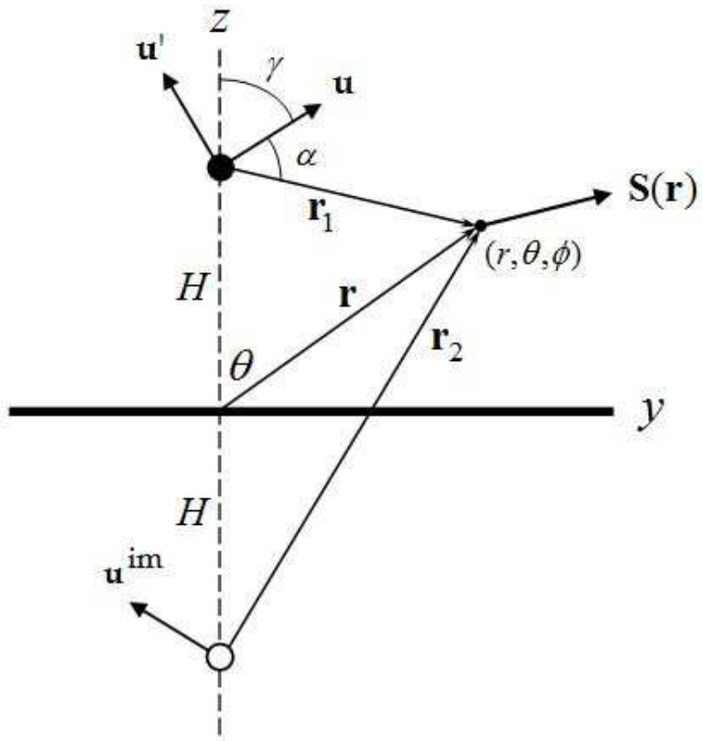


Fig. 13. Setup of the dipole near the mirror.

The vortices and singularities in Figs. (14) and (15) are a result of interference between the radiation that is emitted by the dipole and the radiation that is reflected off the surface. Close to the dipole, the field that is emitted directly by the dipole is much stronger than the reflected field, and it may seem that therefore this field dominates the energy flow pattern.

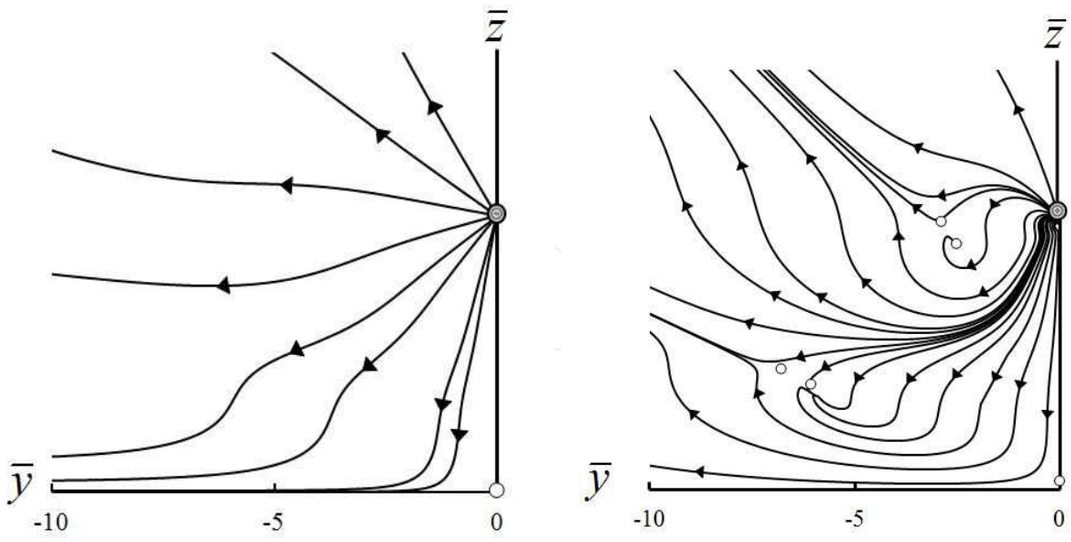


(a) (b)

Fig. 14. The figure on the left shows the field line pattern for a dipole oscillating perpendicular the the surface. Field lines that are headed towards the surface bend when they come close to the surface. For the figure on the right, the dipole oscillates parallel to the surface, and we see the appearance of singularities. The distance between the dipole and the interface is one wavelength for both figures ( $h = 2\pi$ ).

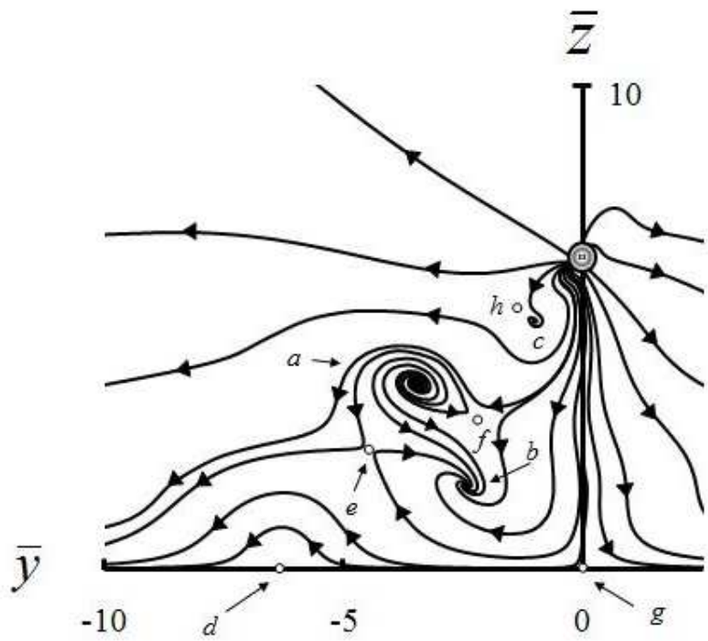


Fig. 15. Field line pattern for a dipole oscillating under 45° with the $z$ axis, and for $h = 2\pi$ . Numerous singularities are present, and three vortices appear.

In other words, we may expect that close to the dipole the field lines are straight lines, as in Fig. 1(a), and that away from the dipole interference sets in, leading to complicated flow patterns as in Figs. (14) and (15). We shall now show that this is not the case. In order to study the emission of the radiation, we consider a region close to the dipole. We assume $q_1 << 1$ and $q_1 << h$. This means that we consider field points that are close to the dipole, compared to a wavelength, and we assume that the distance between the mirror and the dipole is much larger than the distance between the dipole and the field point. The expression for the Poynting vector can be expanded in a series in $q_1$, and we obtain

$$\boldsymbol{\sigma}(\mathbf{q}) = \frac{\sin\gamma}{q_1} v(h)[(3\cos^2\alpha - 1)\mathbf{u}' - 3\cos\alpha(\hat{\mathbf{q}}_1 \cdot \mathbf{u}')\mathbf{u}] + \hat{\mathbf{q}}_1 \sin^2\alpha + O(1) \tag{79}$$

Here, $\alpha$ is the angle between $\mathbf{u}$ and $\hat{\mathbf{q}}_1$, vector $\mathbf{u}'$ is defined as

$$\mathbf{u}' = -\mathbf{e}_y \cos\gamma + \mathbf{e}_z \sin\gamma \ , \tag{80}$$

and

$$v(h) = \frac{1}{2h}\left[\frac{\sin(2h)}{2h} - \cos(2h)\right] \tag{81}$$

Without the mirror, this would be $\boldsymbol{\sigma}(\mathbf{q}) = \hat{\mathbf{q}}_1 \sin^2\alpha$, and this is exact at all distances. The corresponding field lines are straight, as in Fig. 1(b). Due to interference, the first term in

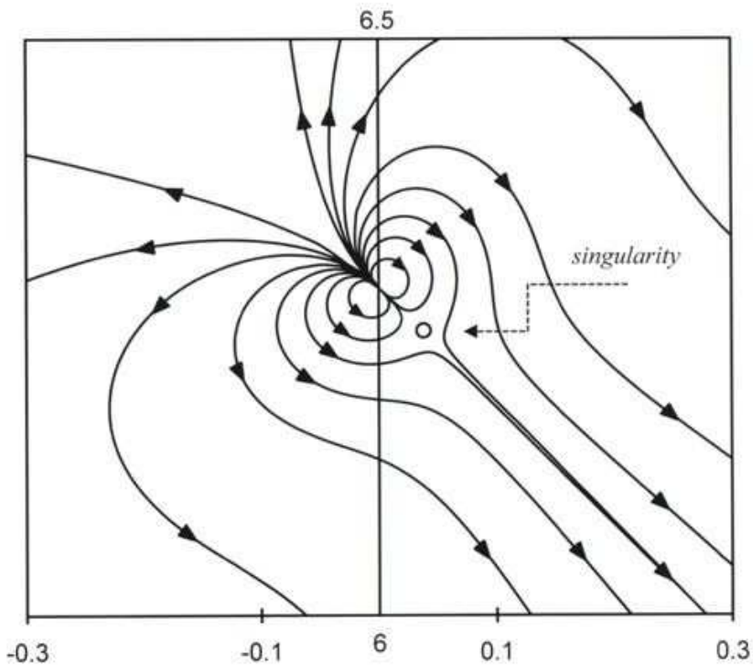


Fig. 16. Field line pattern close to the dipole for $\gamma = 45^\circ$ and $h = 2\pi$.

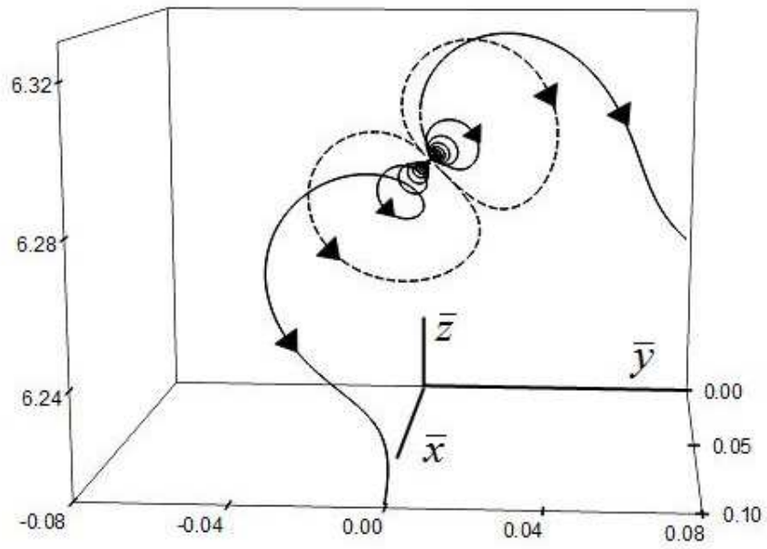


Fig. 17. Field line pattern close to the dipole for $\gamma = 45^\circ$ and $h = 2\pi$ , in 3D. It appears that the radiation is emitted as a set of four vortices.

(79) appears, and this term is proportional to $1/q_1$. Close to the dipole, this term dominates. The field line picture close to the dipole is shown in Fig. 16. We see that some field lines are closed loops, and a singularity appears very close to the dipole. When we graph the field lines in 3D, we obtain the result shown in Fig. 17. In front of the *yz* plane, there are two vortices which come out of the dipole. Two other vortices are behind the *yz* plane, but these are not shown in the figure. The dashed curves in the figure are closed loops from Fig. 16 in the *yz* plane. Therefore, radiation is emitted as a set of four vortices, and this is a result of interference between the directly emitted radiation and the reflected field by the mirror. These vortices are present no matter the distance between the dipole and the mirror, but the spatial extent of the vortices diminishes with distance.

## 12. Conclusions

Energy in an electromagnetic field flows along the field lines of the Poynting vector. We have considered the radiation emitted by an electric dipole. For a linear dipole in free space, the field lines are straight lines coming out of the dipole. When the dipole moment rotates in the *xy* plane, the field lines are curves that lie on cones around the z axis. Close to the source, the field lines wind around the *z* axis a large number of times, and at larger distances, in the far field, the field lines approach asymptotically straight lines. Such a line is displaced, as compared to a line that would start at the location of the dipole, and this gives a virtual displacement of the position of the source in the *xy* plane. Also in the far field, this line is displaced as compared with the radially outward direction, and this gives rise to a shift of the image of the dipole when projected onto an observation plane. When the dipole is embedded in a medium, the damping in the material gives rise to a redistribution of the power flow, as compared to emission in free space. For a linear dipole, the field lines are not

straight anymore, and for a circular dipole a field line has a funnel appearance, rather than lying on a cone. Also the spacing of the field lines near the source becomes much less dense due to the damping. It is also shown that when the real part of the permittivity is negative, the field lines reverse in rotation direction, and the flow of energy counterrotates the rotation direction of the dipole. The virtual displacement of the location of the source and the displacement of the image in the far field can be much larger than in free space. When the dipole is located near the surface of a mirror, a host of new phenomena appear due to the interference of the dipole radiation with the reflected radiation by the mirror. In the flow field, singularities and vortices appear in the neighborhood of the dipole and in between the dipole and the mirror. For a linear dipole in free space, the field lines come straight out of the dipole, but when this dipole is located near a mirror, the mechanism of emission is drastically altered. In the oscillation plane of the dipole, all radiation is emitted in a direction perpendicular to the dipole moment, and some field lines form closed loops. Energy flowing along these field lines returns to the dipole. For emission off this plane, the radiation is emitted as a set of four vortices, emanating from the dipole.

## 13. References


Arnoldus, H. F. & Foley, J. T. (2004), The dipole vortex, *Optics Communications*, Vol. 231, No. 1, (Feb. 2004) (115-128), ISSN: 0030-4018.

Born, M. & Wolf, E. (1980). *Principles of Optics* (6th edition), Pergamon, ISBN: 0-08-026482-6, Oxford, Ch. 3.

Haefner, D., Sukhov, S. & Dogariu, A. (2009), Spin-Hall effect of light in spherical geometry, *Physical Review Letters*, Vol. 102, No. 12, (Mar. 2009) (123903-1-123903-4), ISSN: 0031-9007.

Jackson, J. D. (1998). *Classical Electrodynamics* (3rd edition), Wiley, ISBN: 0-471-30932-X, New York, p. 265.

Li, X. & Arnoldus, H. F. (2010a), Macroscopic far-field observation of the sub-wavelength near-field dipole vortex, *Physics Letters A*, Vol. 374, No. 8, (Feb. 2010) (1063-1067), ISSN: 0375-9601.

Li, X. & Arnoldus, H. F. (2010b), Electric dipole radiation near a mirror, *Physical Review A*, Vol. 81, No. 5, (May 2010) (053844-1-053844-10), ISSN: 1050-2947.

Li, X. & Arnoldus, H. F. (2010c), Reversal of the dipole vortex in a negative index of refraction material, *Physics Letters A*, Vol. 374, No. 43, (Sep. 2010) (4479-4482), ISSN: 0375-9601.

Li, X., Pierce, D. M. & Arnoldus, H. F. (2011a), Redistribution of energy flow in a material due to damping, *Optics Letters*, Vol. 36, No. 3, (Feb. 2011) (349-351), ISSN: 0146-9592.

Li, X., Pierce, D. M. & Arnoldus, H. F. (2011b), Damping of the dipole vortex, *Journal of the Optical Society of America A*, Vol. 28, No. 5, (May 2011) (778-785), ISSN: 1084-7529.

McCall, M. W., Lakhtakia, A. & Weiglhofer, W. S. (2002), The negative index of refraction demystified, *European Journal of Physics*, Vol. 23, No. 3, (May 2002) (353-359), ISSN: 0143-0807.

Shu, J., Li, X. & Arnoldus, H. F. (2008), Energy flow lines for the radiation emitted by a dipole, *Journal of Modern Optics*, Vol. 55, No. 15, (Sep. 2008) (2457-2471), ISSN: 0950-0340.

Shu, J., Li, X. & Arnoldus, H. F. (2009), Nanoscale shift of the intensity distribution of dipole radiation, *Journal of the Optical Society of America A*, Vol. 26, No. 2, (Feb. 2009) (395-402), ISSN: 1084-7529.

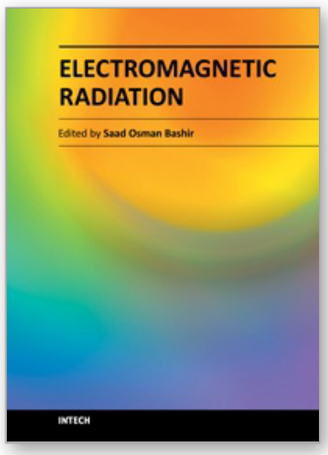


**Electromagnetic Radiation**

Edited by Prof. S. O. Bashir

ISBN 978-953-51-0639-5
Hard cover, 288 pages
**Publisher** InTech
**Published online** 05, June, 2012
**Published in print edition** June, 2012

The application of electromagnetic radiation in modern life is one of the most developing technologies. In this timely book, the authors comprehensively treat two integrated aspects of electromagnetic radiation, theory and application. It covers a wide scope of practical topics, including medical treatment, telecommunication systems, and radiation effects. The book sections have clear presentation, some state of the art examples, which makes this book an indispensable reference book for electromagnetic radiation applications.

**How to reference**

In order to correctly reference this scholarly work, feel free to copy and paste the following:

X. Li, D.M. Pierce and H.F. Arnoldus (2012). Vortices in Electric Dipole Radiation, Electromagnetic Radiation, Prof. S. O. Bashir (Ed.), ISBN: 978-953-51-0639-5, InTech, Available from: http://www.intechopen.com/books/electromagnetic-radiation/vortices-in-electric-dipole-radiation

INTECH
open science | open minds

**InTech Europe**
University Campus STeP Ri
Slavka Krautzeka 83/A
51000 Rijeka, Croatia
Phone: +385 (51) 770 447
Fax: +385 (51) 686 166
www.intechopen.com

**InTech China**
Unit 405, Office Block, Hotel Equatorial Shanghai
No.65, Yan An Road (West), Shanghai, 200040, China
中国上海市延安西路65号上海国际贵都大饭店办公楼405单元
Phone: +86-21-62489820
Fax: +86-21-62489821

IntechOpen